
STRENGTH
AND PLASTICITY

Rolling Textures in BCC Metals: A Biaxial Stress Texture Theory and Experiments

F. Z. Xia^a, H. B. Sun^b, and H. G. Wei^c *

^a School of Mechanical and Electrical Engineering, Jiangxi University of Science and Technology, Ganzhou, 341000 China

^b Capital Aerospace Machinery Corporation Limited, Beijing, 100000 China

^c Faculty of Materials Metallurgy and Chemistry, Jiangxi University of Science and Technology, Ganzhou, 341000 China

*e-mail: weihaigen@jxust.edu.cn

Received May 4, 2020; revised February 23, 2021; accepted February 28, 2021

Abstract—Mechanical properties, such as the tensile anisotropy, of bcc metal sheets are significantly influenced by their rolling textures, so it is important to investigate the texture formation mechanisms in the metals in order to control their textures. A biaxial stress texture theory, which can be used to reveal the texture formation mechanism in bcc metal sheets by analyzing the grain rotation during rolling,—is put forward in this work. With the theory, rolling textures and deformation microstructures in W sheets are studied and it is demonstrated that two stable texture components, namely, (001)[110] and (111)[$\bar{1}0$] textures, are formed in the W sheet rolled to a large reduction (92.4%). The two textures can be converted between each other under the action of conjugate slips and cross slip, leading them to be the stable orientations in the W sheets. The deformation microstructures in the W sheets are investigated by trace analysis in a pole figure based on the biaxial stress texture theory, which shows a consistency between the predictions of the theory and experimental results.

Keywords: rolling texture, texture transformation, deformation microstructure

DOI: 10.1134/S0031918X21070115

INTRODUCTION

Textures in metal sheets have a significant influence on their mechanical anisotropy and workability (such as the deep drawability) [1–4], so it is of practical importance to study the formation mechanisms of rolling textures in metals. In the literature, with regard to the rolling textures in bcc metals, some researchers have focused on modeling the texture formation processes based on the slip system analysis [5–9]. A 90° rotation relationship has been found between the rolling and shear textures in cubic metals, which was explained with the symmetry of the slip systems in cubic metals [9]. Analysis based on a pole figure (PF), which is a powerful modeling tool for slip mechanism analysis, should play an effective role in modeling and interpreting the experimental results if applied. Texture transformations in metals during deformation have been investigated quantitatively [4, 10, 11], of which one of the most remarkable research was conducted by Dillamore [10] who studied the texture transformation during rolling from the crystal-rotation viewpoint on the basis of rolling stress determination utilizing PFs. However, the algorithm for his model and related analytical methods were not presented in detail, impeding the application of his theory. In a metal sheet, a correspondence can often be

found between the rolling texture and special deformation microstructure [12–14]. However, a combined analysis of them based on the texture formation mechanism has been paid little attention. In this work an analytical method and related algorithm are provided for studying the crystal rotation by PFs during rolling. Based on this, the slip mechanism from the {100}<011> type texture to the {111}<100> type texture in W sheets, which are two stable orientations in bcc metal sheets [15, 16], is revealed and related deformation microstructures is analyzed referring to the slip mechanism.

MATERIALS AND METHODS

W sheets used in this work for texture determination were prepared as follows. First, the 22 mm thick W ingots prepared by powder metallurgy were hot rolled at 1500°C to a reduction of 40% through 3 passes, and then they were rolled at 1200°C to a reduction of 92.3% through 8 passes. Microstructures and textures of the rolled W sheets were characterized using EBSD analysis on the rolling direction-normal direction (RD-ND) surfaces of the W sheets. Samples for EBSD examination were prepared by mechanical grinding and electro-polishing in a 2 wt % NaOH solution at room temperature at a constant voltage of 12 V for 1 min. For EBSD characterization, the JSM-5600LV

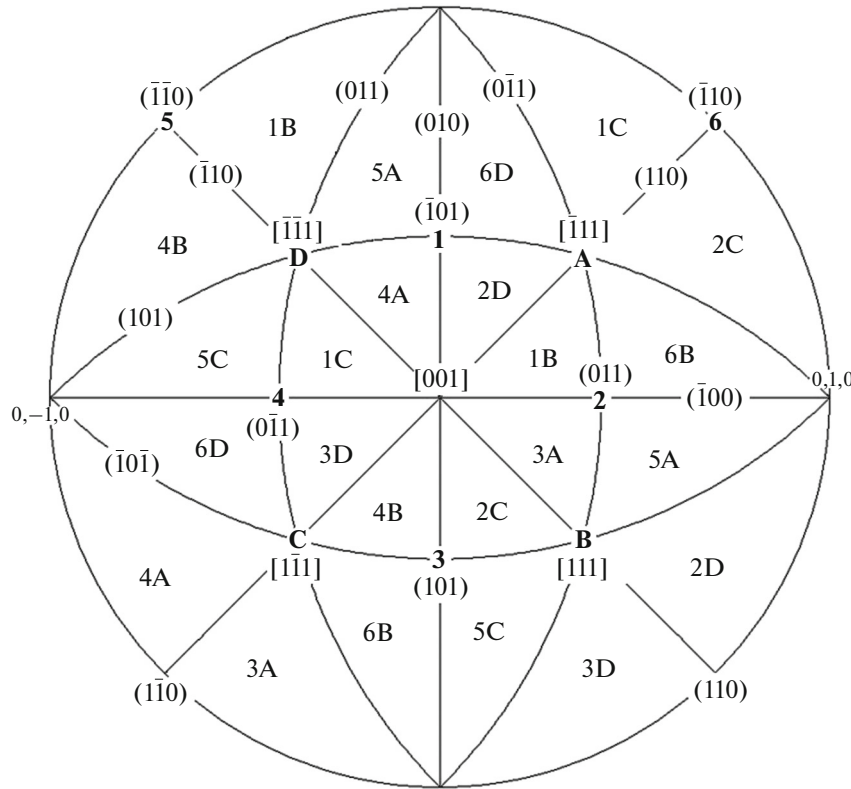


Fig. 1. Standard PF of bcc metals viewed along the [001] direction, see text for notation.

field emission gun of an SEM microscope equipped with the HKL EBSD systems was used and the results were analyzed by HKL Channel 5 software. The crystal rotation occurring during rolling was theoretically investigated as follows. First based on the initial orientation of a grain established by EBSD experiment, the rotation axis and angle were computed using the biaxial stress texture theory proposed in this paper, then the moving trajectories of the poles of RD, transverse direction (TD) and rolling stress direction (RSD) of the rolled sheet were drawn in a PF with the CaRIne Crystallography software based on the knowledge of rotation axis and angle. According to the drawn trajectories, the texture transformations and deformation microstructures in the W sheets were analyzed.

RESULTS AND DISCUSSION

The Biaxial Stress Texture Theory

In Fig. 1 the PF of bcc metals viewed along the [001] direction is shown, in which the following slip elements are indicated.

- (1) poles of the 4 close-packed directions marked with A, B, C, and D;
- (2) poles of the normals of 6 closed-packed planes marked with 1, 2, 3, 4, 5, and 6;

- (3) traces of the 6 closed-packed planes, marked with (011), (0 $\bar{1}$ 1), (110), ($\bar{1}$ 10), (101), and ($\bar{1}$ 01).

In bcc metals there are 12 close-packed slip systems, i. e., 1B, 1C, 2C, 2D, 3A, 3D, 4A, 4B, 5A, 5C, 6B, and 6D slip systems. The PF in Fig. 1 is divided into 24 unit triangles and the slip systems with the maximum shear stress for a rolling stress in any one of the unit triangles are indicated. When the rolling stress locates near or on an adjacent edge between two triangles, the conjugate slip systems indicated in the two triangles will be activated [17].

The rolling stress in a grain can be resolved approximately into a tensile component σ_t parallel to RD and a compressive component σ_c parallel to ND of the rolled sheet, so a vector along σ_t in a grain with an orientation of $(hkl)[uvw]$, i. e., the (hkl) plane of the grain is parallel to the rolling plane and the $[uvw]$ direction is parallel to the RD of the rolled sheet, can be determined as follows.

The unit vector \mathbf{V}_n along ND of the rolled sheet can be determined as

$$\mathbf{V}_n = \frac{h}{\sqrt{h^2 + k^2 + l^2}} \mathbf{a} + \frac{k}{\sqrt{h^2 + k^2 + l^2}} \mathbf{b} + \frac{l}{\sqrt{h^2 + k^2 + l^2}} \mathbf{c}. \quad (1)$$

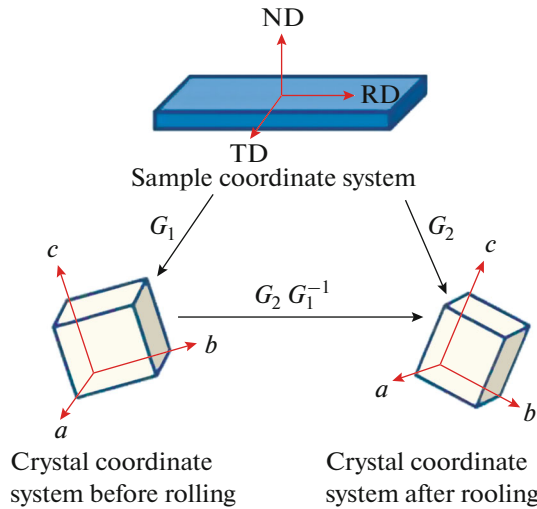


Fig. 2. Schematic illustration of the matrix representations of the rotation relationships between the crystal coordinate systems before and after rolling and the sample coordinate system.

where the vectors **a**, **b**, and **c** are the unit vectors along the crystal coordinate axes. The unit vector \mathbf{V}_r along RD can be determined as

$$\mathbf{V}_r = \frac{u}{\sqrt{u^2 + v^2 + w^2}} \mathbf{a} + \frac{v}{\sqrt{u^2 + v^2 + w^2}} \mathbf{b} + \frac{w}{\sqrt{u^2 + v^2 + w^2}} \mathbf{c}. \quad (2)$$

Then the vector \mathbf{V}_{rs} along RSD can be determined as

$$\mathbf{V}_n = \frac{-h}{\sqrt{h^2 + k^2 + l^2}} + \frac{-u}{\sqrt{u^2 + v^2 + w^2}} \mathbf{a} + \left(\frac{-k}{\sqrt{h^2 + k^2 + l^2}} + \frac{-v}{\sqrt{u^2 + v^2 + w^2}} \right) \mathbf{b} + \left(\frac{-l}{\sqrt{h^2 + k^2 + l^2}} + \frac{-w}{\sqrt{u^2 + v^2 + w^2}} \right) \mathbf{c}. \quad (3)$$

So the activated slip systems in the grain can be determined referring to the position of the vector \mathbf{V}_{rs} in the PF shown in Fig. 1, and then the orientation of the grain rotated to accompany the slips can be determined according to the principles as follows. With the activated slip systems, the slip planes in the grain will rotate to be parallel to the rolling plane, and the slip directions will rotate to be parallel to RD. If a conjugate slip system is activated, the crystal plane of which the index can be **b** determined as the sum of the plane indexes of the conjugate slip systems will rotate to be parallel to the rolling plane, and the crystal direction of which the index can be determined as the sum of the direction indexes of the conjugate slip systems will rotate to be **a** parallel to RD. In the following a method for computing the rotation axis and angle by

which a grain rotates as is described above will be given.

The grain orientation before the rotation can be represented as a matrix

$$\mathbf{G}_1 = \begin{pmatrix} u_1 & r_1 & h_1 \\ v_1 & s_1 & k_1 \\ w_1 & t_1 & l_1 \end{pmatrix}, \quad (4)$$

where $[u_1 \ v_1 \ w_1]$ represents the unit vector along RD, $[r_1 \ s_1 \ t_1]$ the unit vector along TD, and $[h_1 \ k_1 \ l_1]$ the unit vector along ND. The three unit vectors are expressed in the crystal coordinate system. For matrix \mathbf{G}_1 an equation can be written as

$$\begin{pmatrix} u_1 & r_1 & h_1 \\ v_1 & s_1 & k_1 \\ w_1 & t_1 & l_1 \end{pmatrix} \times \begin{pmatrix} 1 & 0 & 0 \\ 0 & 1 & 0 \\ 0 & 0 & 1 \end{pmatrix} = \begin{pmatrix} u_1 & r_1 & h_1 \\ v_1 & s_1 & k_1 \\ w_1 & t_1 & l_1 \end{pmatrix}, \quad (5)$$

where the three unit column vectors in the second matrix can be regarded as the three vectors along the crystal coordinate axes. According to the matrix expression corresponding to a crystal rotation, \mathbf{G}_1 is also the rotation matrix by which the crystal coordinate system can be rotated to the initial orientation of the sample coordinate system before rolling.

It is assumed that the grain orientation after rolling, which is named the goal orientation here, can be represented as a matrix

$$\mathbf{G}_2 = \begin{pmatrix} u_2 & r_2 & h_2 \\ v_2 & s_2 & k_2 \\ w_2 & t_2 & l_2 \end{pmatrix}, \quad (6)$$

where $[u_2 \ v_2 \ w_2]$ is the unit vector along RD, $[r_2 \ s_2 \ t_2]$ the unit vector along TD, and $[h_2 \ k_2 \ l_2]$ the unit vector along ND. The three unit vectors are expressed in the crystal coordinate system. Matrix \mathbf{G}_2 is also the rotation matrix by which the goal orientation of the sample coordinate system can be rotated to the crystal coordinate system. On the other hand, according to the above definition, \mathbf{G}_1^{-1} is the rotation matrix by which the initial sample coordinate system before rolling can be rotated to the crystal coordinate system. So the rotation matrix by which the sample coordinate system before rolling can be rotated to the goal orientation of the sample coordinate system after rolling can be obtained as

$$\mathbf{G} = \mathbf{G}_2 \mathbf{G}_1^{-1}. \quad (7)$$

Furthermore, it can be obtained that $\mathbf{G}_1^1 = \mathbf{G}_1^T$, because matrix \mathbf{G}_1 consists of three unit vectors which are perpendicular to one another [18], so matrix \mathbf{G} can be determined as

$$\mathbf{G} = \mathbf{G}_2 \mathbf{G}_1^T. \quad (8)$$

The matrix representations of the rotations between the different coordinate systems described above are schematically illustrated in Fig. 2.

According to the theory of coordinate rotation [19], the rotation angle θ and axis R of the rotation represented by matrix \mathbf{G} can be determined as

$$\theta = \cos^{-1} \left(\frac{G_{11} + G_{22} + G_{33} - 1}{2} \right), \quad (9)$$

$$\text{and } R = \left(\frac{G_{23} - G_{32}}{2\sin\theta}, \frac{G_{31} - G_{13}}{2\sin\theta}, \frac{G_{12} - G_{21}}{2\sin\theta} \right) \quad (10)$$

respectively, for which G_{ij} is the element in matrix \mathbf{G} in the i th row and the j th column. In Eq. (10) the rotation axis is expressed in the crystal coordinate system. Based on the rotation axis and angle, the rotation trajectories of RSD, ND, and RD on a PF can be drawn using the CaRIne Crystallography 3.1 software and then activated slip systems and texture transformation can be analyzed.

In the theory proposed above, the vector along RSD in a grain is determined utilizing the directions of RD and ND, so the theory is named the biaxial stress texture theory.

Application of the Biaxial Stress Texture Theory

ND inverse pole figures (IPFs) and $\psi_2 = 45^\circ$ ODF sections of Orientation Distribution Function of the W sheets rolled to the reductions of 50 and 92.4% are shown in Fig. 3. It can be determined from Fig. 3b that (001)[110], (001)[0 $\bar{1}$ 0], (111)[1 $\bar{1}$ 0], and (111)[1 $\bar{2}$ 1] textures are formed in the W sheet rolled to the reduction of 50%. Furthermore, the grain orientations in the W sheet are distributed mainly around the four textures at this deformation stage. After the W sheet is rolled to the reduction of 92.4%, both the (001)[110] and (111)[1 $\bar{1}$ 0] textures are reinforced whereas other textures are weakened significantly, as is shown in Fig. 3d.

In Figs. 4a, 4b the ND and RD RPFs of a grain near the (001)[110] orientation in the W sheet hot rolled to the reduction of 50% are shown, respectively. In Figs. 4c, 4d (101) and (111) PFs of regions A and B in Fig. 4a are shown, respectively. The green and blue points on the two PFs denote the orientations of regions A and B in Fig. 4a, respectively. It is determined with the HKL software that the orientation of region A is (001)[$\bar{1}$ 5 16 0], which is near the (001)[$\bar{1}$ 10] texture orientation. The orientation is (20 $\bar{5}$ 1) [3, 10, 10] for region B, indicating a crystal rotation between the regions A and B. This should be attributed to the crystal slip occurred during rolling, which can induce a texture transformation at the same time. In the following this orientation transformation will be analyzed based on the biaxial stress texture theory.

The orientation of region A in Fig. 4a can be represented by a matrix according to Eq. (4) as

$$\mathbf{G}_1 = \begin{pmatrix} -0.68 & 0.73 & 0 \\ 0.73 & 0.68 & 0 \\ 0 & 0 & 1 \end{pmatrix}. \quad (11)$$

A vector along RSD in region A can be determined according to Eq. (3) as [0.68 0.73 $\bar{1}$], the pole of which is indicated by a red point on the PF in Fig. 5. Compared with Fig. 1 it can be determined that at this orientation of RSD, the conjugate slip systems of 2D(011)[$\bar{1}$ $\bar{1}$ 1] + 1B($\bar{1}$ 01)[111] will be activated in region A, under which region A will rotate to the orientation ($\bar{1}$ 12)[110] which can be expressed by a matrix as

$$\mathbf{G}_2 = \begin{pmatrix} -0.06 & -0.91 & -0.41 \\ -0.90 & -0.12 & 0.41 \\ 0.42 & 0.39 & 0.82 \end{pmatrix}. \quad (12)$$

According to Eqs. (7)–(9) the rotation axis and angle by which region A is rotated can be determined based on matrix \mathbf{G}_1 in Eq. (11) and \mathbf{G}_2 in Eq. (12) as (0.01 0.42 0.91) and 93.58° , respectively. The rotation trajectories of the poles of RD, ND, and RSD are drawn in Fig. 5 with a rotation angle interval of 5° between adjacent points on the trajectories using the CaRIne Crystallography software. The arrows in Fig. 5 indicate the rotation directions. It can be seen that during the rotation RSD will go over the trace of (01 $\bar{1}$) plane, stimulating the slip system 6D ($\bar{1}$ 10)[$\bar{1}$ 11] which is the cross slip system of 2D slip system. The cross slips occurred during deformation can relax work hardening [20–22], so when RSD in region A rotates to near the trace of (01 $\bar{1}$) plane it is energetically favorable for the multiple slip systems of 2D + 1B + 6D to be activated. Under the multiple slips, for the orientation ($\bar{1}$ 12)[110] to which region A tends to rotate to under the action of conjugate slips of 2D + 1B, ($\bar{1}$ 12) crystal plane in the orientation will be transformed to ($\bar{1}$ 11) plane as a result of the activation of slip system 6D, without the crystal direction [110] being changed, because both slip directions of systems 2D and 6D are [$\bar{1}$ $\bar{1}$ 1]. It means that a texture transformation from (001)[110] to ($\bar{1}$ 11)[110] occurs. In a similar way, a texture transformation from ($\bar{1}$ 11)[110] to (001)[110] can also be caused under the action of conjugate slip and cross slip, which can be derived also using the biaxial stress texture theory. It means that the two textures can only be transformed to each other, other than being eliminated during rolling after they are formed in the rolled sheets. This is why ($\bar{1}$ 11)[110] and (001)[110] textures are the two stable orientations

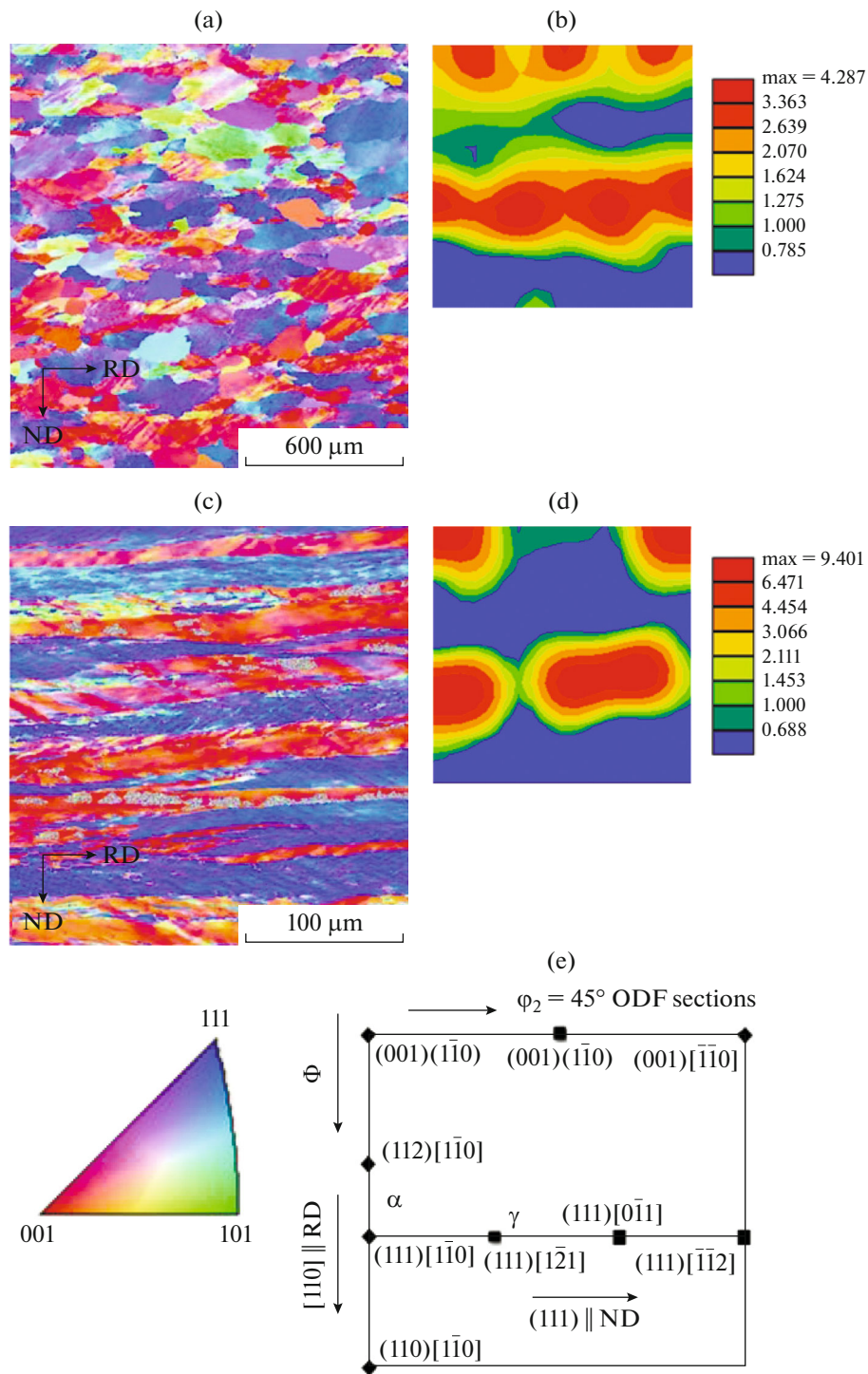


Fig. 3. (a) and (b) are the ND IPF and $\psi_2 = 45^\circ$ ODF section of the W sheet rolled to the reduction of 50%, respectively; (c) and (d) are the ND IPF and $\psi_2 = 45^\circ$ ODF section of the W sheet rolled to the reduction of 92.4%, respectively; (e) $\psi_2 = 45^\circ$ ODF section of bcc metals.

in the W sheets rolled to the large reduction, as shown in Fig. 3d.

It can be determined from matrix \mathbf{G}_1 in Eq. (11) that TD of region A in Fig. 4a is approximately parallel

to the $[110]$ direction. Viewed along this direction, the slip plane traces of slip systems 2D, 1B, and 6D can be drawn on a PF, as shown in Fig. 6a (dashed lines). It can be seen that the slip plane traces of slip systems 2D and 1B are parallel to each other, and the angles

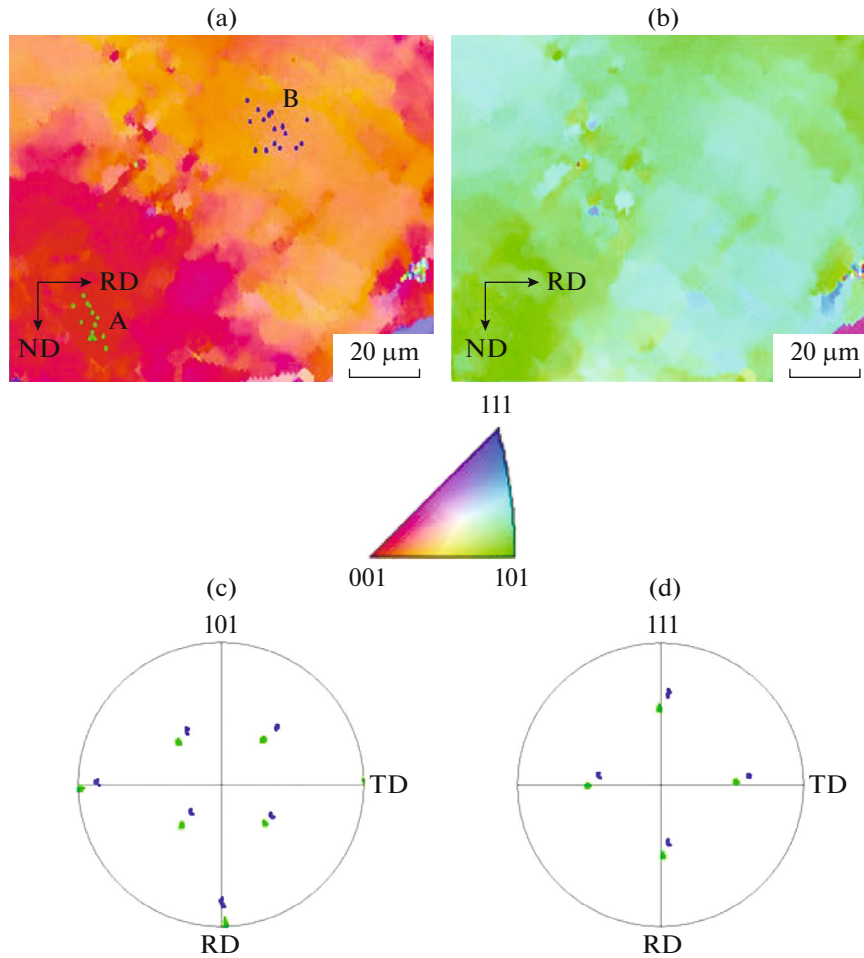


Fig. 4. (a) ND and (b) RD RPFs of a grain of near the (001)[110] orientation in the W sheet rolled to the reduction of 50%, respectively; (c) (101) and (d) (111) PFs of regions A and B in (a), respectively. On the two PFs, the green and blue points denote the orientations of regions A and B, respectively in (a).

between the slip plane traces of systems 1B and 6D and 2D and 6D are both 60°, respectively. In Fig. 6b all the {110} plane traces determined by the EBSD software analysis of region A in Fig. 4a are indicated by blue lines on the quality figure of region A. In the quality figure the main deformation microstructure boundaries formed in region A are also marked by the red dashed lines. It can be seen that two deformation microstructure boundaries are formed in region A, between which the angle is about 61.5° which is approximately equal to the angle between the slip plane traces indicated in Fig. 6a. It can be seen in Fig. 6b that the deformation microstructure boundaries are also approximately parallel to any one of the {110} plane traces indicated by the blue lines, demonstrating that the activated slip systems in region A should be the multiple slip systems 2D + 1B + 6D. This indicating that the slip systems predicted by the biaxial stress texture theory are in accordance with the actual case.

It is determined above that the grain in region A in Fig. 4a will be rotated to the orientation $(\bar{1}11)[101]$

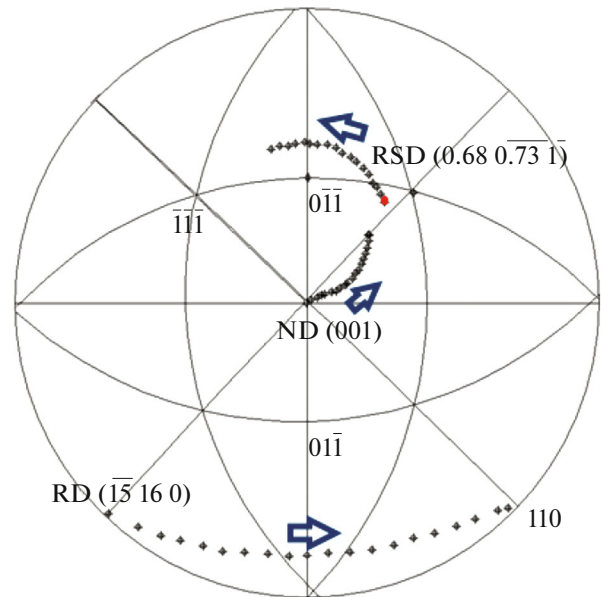


Fig. 5. The trajectories of RD, ND, and RSD of region A in Fig. 4 under the action of conjugate slip systems of 2D + 1B.

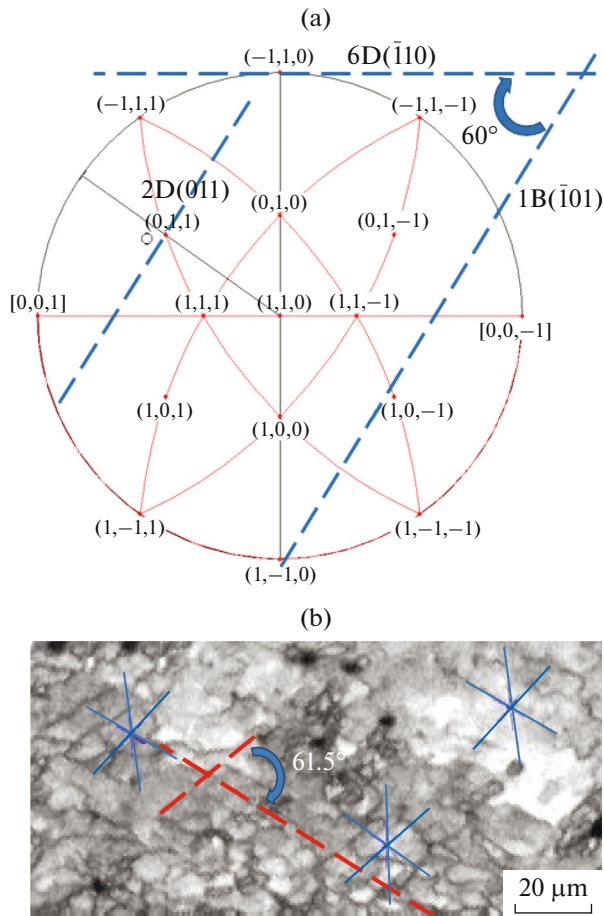


Fig. 6. (a) The slip plane traces (blue dashed lines) of slip systems 2D, 1B, and 6D of region A in Fig. 4a on the PF viewed along the $[110]$ direction; (b) the quality image of region A in Fig. 4a, in which the blue lines indicate the traces of $\{110\}$ planes in the pointed positions and the red dashed lines indicate the main deformation microstructure boundaries in the image. It can be seen that a red dashed line is approximately parallel to one of the blue lines in the figure.

under the action of multiple slip systems $2D + 1B + 6D$, then the rotation matrix can be determined according to Eqs. (4)–(9) as

$$\mathbf{G} = \begin{pmatrix} -0.78 & 0.24 & -0.58 \\ -0.60 & -0.56 & 0.58 \\ -0.19 & 0.80 & 0.58 \end{pmatrix}. \quad (13)$$

Based on the rotation matrix \mathbf{G} , it can be determined according to Eqs. (9) and (10) that the rotation axis is $(0.23 \ 0.41 \ 0.88)$ and rotation angle 29.2° , based on which the trajectories of $\{111\}$ and $\{110\}$ poles of region A in Fig. 4a can be drawn on a PF viewed along the TD direction, as shown in Fig. 7. It can be seen that the trajectories of these poles predicted with the biaxial stress texture theory are almost consistent with

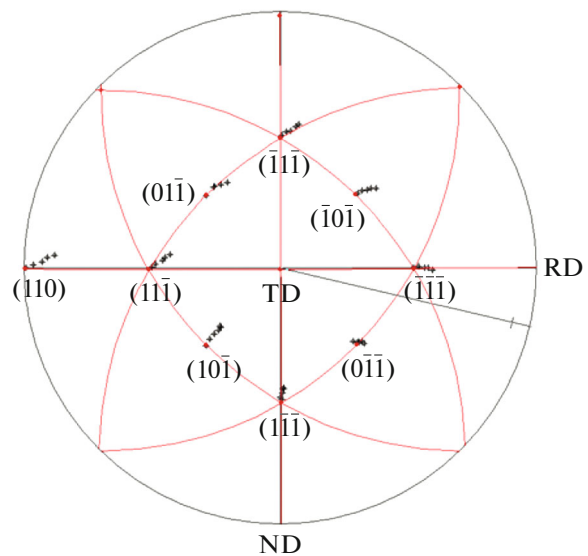


Fig. 7. Predicted trajectories of $\{111\}$ and $\{110\}$ poles of region A in Fig. 4a based on the activation of multiple slips $2D + 1B + 6D$ viewed along the TD direction, with a 1° angle interval between adjacent crosses.

the shifts of the poles of region B compared with region A observed practically in Figs. 4c, 4d, indicating that the biaxial stress texture theory can make a reasonable prediction on the crystal rotation during rolling, and region B should be the transitional orientation of region A transformed to the orientation $(\bar{1}11)[101]$.

CONCLUSIONS

Based on the matrix representation of crystal rotation during rolling, a biaxial stress texture theory is proposed in this work. The crystal rotation and hence the texture formation mechanisms in bcc metals are analyzed on PFs with the theory. EBSD experimental results demonstrate that $(001)[110]$, $(001)[0\bar{1}0]$, $(111)[1\bar{1}0]$, and $(111)[1\bar{2}1]$ textures are formed in the W sheet rolled to the reduction of 50%, whereas only $(001)[110]$ and $(111)[1\bar{1}0]$ components are retained and reinforced after the W sheet is rolled to the reduction of 92.4%. Theoretical analysis with the texture theory demonstrates that the two textures can be transformed between each other under the action of conjugate slips and cross slip, leading them to be the stable orientations in the rolled W sheets. Based on the trace analysis on PFs, the deformation microstructure boundaries and crystal rotations are studied, demonstrating the consistency between the theoretical predictions and experimental results and hence the validity of the biaxial stress texture theory.

FUNDING

This research was funded by “Young People Fund of Jiang Xi province, grant number 2018BAB216005” and “Jiang Xi province ministry of education, grant numbers GJJ180469 and GJJ17056.”

REFERENCES

1. Y. Yoshihiro, O. Yoshihiro, K. Yasushi, and F. Osamu, “Development of ferritic stainless steel sheets with excellent deep drawability by {1 1 1} recrystallization texture control,” *JSAE Rev.* **24**, No. 4, 483–488 (2003).
2. S. R. Agnew and J. R. Weertman, “The influence of texture on the elastic properties of ultrafine-grain copper,” *Mater. Sci. Eng., A* **242**, No. 1, 174–180 (1998).
3. H. R. Wenk and P. Van Houtte, “Texture and anisotropy,” *Rep. Prog. Phys.* **67**, No. 8, 1367–1428 (2004).
4. L. A. I. Kestens and H. Pirgazi, “Texture formation in metal alloys with cubic crystal structures,” *Mater. Sci. Technol.* **32**, No. 13, 1303–1315 (2016).
5. J. L. Raphanel and P. Van Houtte, “Simulation of the rolling textures of b.c.c. metals by means of the relaxed taylor theory,” *Acta. Metall.* **33**, No. 8, 1481–1488 (1985).
6. S. H. Lee and D. N. Lee, “Modelling of Deformation Textures of Cold Rolled BCC Metals by the Rate Sensitivity Model,” *Key Eng. Mater.* **177–180**, 115–120 (2000).
7. B. L. Hansen, J. S. Carpenter, S. D. Sintay, and C. A. Bronkhorst, “Modeling the texture evolution of Cu/Nb layered composites during rolling,” *Int. J. Plast.* **49**, No. 9, 71–84 (2013).
8. N. L. Dong, “Relationship between deformation and recrystallisation textures of fcc and bcc metals,” *Philos. Mag.* **85**, Nos. 2–3, 297–322 (2005).
9. M. Hölscher, D. Raabe, and K. Lücke, “Relationship between rolling textures and shear textures in f.c.c. and b.c.c. metals,” *Acta. Metall. Mater.* **42**, No. 3, 879–886 (1994).
10. I. L. Dillamore and W. T. Roberts, “Rolling textures in f.c.c. and b.c.c. metals,” *Acta. Metall.* **12**, No. 3, 281–293 (1964).
11. M. Hui, J. Du, R. J. Chen, and J. Liu, “Evolution of texture and magnetic property in Nd–Pr–Fe–B based nanocomposite magnets with plastic deformation,” *IEEE. T. Magn.* **51**, No. 11, 1–4 (2015).
12. J. Gil Sevillano, C. García-Rosales, and J. Flaquer Fuster, “Texture and large-strain deformation microstructure,” *Philos. Trans. R. Soc. London, A* **357**, No. 1756, 1603–1619 (1999).
13. B. Hutchinson, “Deformation microstructures and textures in steels,” *Philos. Trans. R. Soc. London, A* **357**, No. 1756, 1471–1485 (1999).
14. C. S. Hong, X. X. Huang, and G. Winther, “Dislocation content of geometrically necessary boundaries aligned with slip planes in rolled aluminum,” *Philos. Mag.* **93**, No. 23, 3118–3141 (2015).
15. B. Ravi Kumar, A. K. Singh, D. Samar, and D. K. Bhattacharya, “Cold rolling texture in AISI 304 stainless steel,” *Mater. Sci. Eng., A* **364**, No. 1, 132–139 (2004).
16. I. L. Dillamore and H. Katoh, “Comparison of the observed and predicted deformation textures in cubic metals,” *Met. Sci.* **8**, No. 1, 21–27 (1974).
17. G. Winther and X. Huang, „Dislocation structures. Part II. Slip system dependence,” *Philos. Mag.* **87**, No. 33, 5215–5235 (2007).
18. L. W. Johnson, R. D. Riess, and J. T. Arnold, *Introduction to Linear Algebra* (Addison-Wesley N.Y., New York, 1989), pp. 256–283.
19. P. Yang, *Electron Backscattering Diffraction Technology and its Application* (Metallurgical Industry Press, Bei Jing, 2007), pp. 235–250.
20. D. C. Hu and M. H. Chen, “Dynamic tensile properties and deformational mechanism of C5191 phosphor bronze,” *Rare. Met. Mater. Eng.* **46**, No. 6, 1518–1523 (2017).
21. B. Peeters, M. Seefeldt, C. Teodosiu, S. R. Kalidindi, P. Van Houtte, and E. Aernoudt, “Work-hardening/softening behaviour of b.c.c. polycrystals during changing strain paths: I. An integrated model based on substructure and texture evolution, and its prediction of the stress–strain behaviour of an IF steel during two-stage strain paths,” *Acta. Mater.* **49**, No. 9, 1607–1619 (2001).
22. K. Máthis, Z. Trojanová, P. Lukáč, C. H. Cáceres, and J. Lendvai, “Modeling of hardening and softening processes in Mg alloys,” *J. Alloy. Compd.* **378**, No. 1, 176–179 (2004).